STRUCTURE OF UNSTEADY PARTIALLY PREMIXED FLAMES AND THE EXISTENCE OF STATE RELATIONSHIPS

Suresh K. Aggarwal (ska@uic.edu)

Mechanical and Industrial Engineering, University of Illinois at Chicago

842 W. Taylor St., Chicago, IL 60607, USA

ABSTRACT

In this study, we examine the structure and existence of state relationships in unsteady partially premixed flames (PPFs) subjected to buoyancy-induced and external perturbations. A detailed numerical model is employed to simulate the steady and unsteady two-dimensional PPFs established using a slot burner under normal and zero-gravity conditions. The coflow velocity is parametrically varied. The methane-air chemistry is modeled using a fairly detailed mechanism that contains 81 elementary reactions and 24 species. Validation of the computational model is provided through comparisons of predictions with nonintrusive measurements. The combustion proceeds in two reaction zones, one a rich premixed zone and the other a nonpremixed zone. These reaction zones are spatially separated, but involve strong interactions between them due to thermochemistry and scalar transport. The fuel is mostly consumed in the premixed zone to produce CO and H_2, which are transported to and consumed in the nonpremixed zone. The nonpremixed zone in turn provides heat and H-atoms to the premixed zone. For the range of conditions investigated, the zero-g partially premixed flames exhibit a stable behavior and a remarkably strong resistance to perturbations. In contrast, the corresponding normal-gravity flames exhibit oscillatory behavior at low coflow velocities but a stable behavior at high coflow velocities. The effects of coflow and gravity on the flames are characterized through a parameter V_R, defined as the ratio of coflow velocity to jet velocity. For $V_R \leq 1$ (low coflow velocity regime), the structures of both 0- and 1-g flames are strongly sensitive to changes in V_R, while they are only mildly affected by coflow in the high coflow velocity regime ($V_R > 1$). In addition, the spatio-temporal characteristics of the 0- and 1-g flames are markedly different in the first regime, but are essentially similar in the second regime. A more significant difference in the first regime between these flames is the presence of a flow instability that manifests itself through the self-excited oscillations of the 1-g flame and the concomitant flickering of the nonpremixed reaction zone. For $V_R \leq 1$, as the coflow velocity is increased, the oscillation amplitude decreases and the oscillation frequency increases, both of which are in accord with previous experimental and computational results concerning 1-g jet diffusion flames. The modified conserved scalar approach is found to be effective in characterizing the flame structure and developing state relationships for both steady and unsteady partially premixed flames. This is demonstrated by the fact that the temperature as well as the major and minor species profiles follow similar state relationships in terms of the modified mixture fraction for the 0- and 1-g flames, even though these flames have markedly different spatio-temporal characteristics.

1. Introduction

Partially–premixed flames are established when less than stoichiometric quantity of oxidizer is molecularly mixed with the fuel stream before entering the reaction zone where additional oxidizer is available for complete combustion. This mode of combustion can be used to exploit the advantages of both nonpremixed and premixed flames regarding operational safety, lower pollutant emissions and flame stabilization. Partial premixing occurs in numerous reacting systems, which include nonpremixed lifted flames, turbulent nonpremixed combustion, spray flames, and unwanted fires.

Partially premixed combustion has been a subject of numerous experimental and theoretical investigations employing both counterflow and coflow configurations. Tsuji and Yamaoka[1,2,3] reported the first comprehensive investigation of such flames. A partially–premixed methane-air flame was established by them in the forward stagnation region of a porous cylinder immersed in a uniform air stream. It was observed that, depending on the stoichiometry of the premixed mixture, the flame contained two spatially separated but interacting reaction zones. The inner premixed reaction zone was established on the cylinder side, and provided CO and H_2 that served as "intermediate fuels" for the outer nonpremixed reaction zone. The latter in return provided heat and radical species (H and OH) to the premixed reaction zone.

Our recent investigations[4,5] focused on partially premixed flames containing two reaction zones in a coflow configuration. Both measurements and simulations were used to examine the detailed structure of methane-air flames stabilized on a Wolfhard-Parker slot burner. Similar to the counterflow configuration, the partially premixed flame in a coflow configuration also contained two reaction zones, namely an inner rich premixed reaction zone

and an outer nonpremixed reaction zone, over a wide range of equivalence ratios and velocities. While the fuel consumption chemistry producing CO and H_2 dominated the inner premixed reaction zone, that in the outer nonpremixed reaction zone was characterized by the CO and H_2 oxidation chemistry. The comparison of predicted and measured flames indicated a direct correlation between the predicted heat release rate contours and the experimentally–obtained C_2^*-chemiluminescent emission contours.

In a subsequent study[6], we investigated steady partially premixed flames established under normal and zero gravity conditions. The results showed that the inner premixed reaction was only mildly affected by gravity, whereas the outer nonpremixed reaction zone was strongly influenced by gravity. Compared to the 0-g case, the 1-g outer reaction zone was taller, more compact, and spatially closer to the inner premixed reaction zone, since the presence of gravity enhanced the advection of air into the outer reaction zone. Investigations of axisymmetric partially premixed flames have been reported by Bennet et al[34]. Recently, we have investigated lifted triple flames and addressed issues related to flame stabilization[7]. We found that both lifted and burner–stabilized flames exhibit remarkable similarity with respect to the shapes and separation distances regarding the three reaction zones. The heat release distribution and the scalar profiles are also virtually identical for lifted and burner stabilized flames in mixture fraction space and attest to the similitude between the burner stabilized and lifted flames.

1.1 Unsteady Partially Premixed Flames

Although the importance of unsteady partially premixed flames has been recognized, the relevant studies are limited. Yule et al.[8] experimentally investigated the transition between laminar and turbulent flames. A double flow structure with inner, fast moving eddies and outer, large, slow moving eddies was observed. There appeared to be no observable correlation or interaction between the inner and outer vortices up to about ten jet diameters ($\xi/D = 10$).

Beyond this position, the outer eddies encroached increasingly into the jet center and there was obviously an interaction between the two instability modes. The flow exhibited an increasing growth of "three-dimensionality" with downstream distance. An increase in the jet equivalence ratio was found to decrease the thickness of the pre-heat zone situated between the inner and outer layers. An examination of Schlieren spectra indicated that the most energetic frequency occurs at lower frequencies as the equivalence ratio was increased, implying that reducing the level of partial premixing decreased the instability frequency. The instability, however, corresponded to the Kelvin-Helmhotz type instability[9] associated with the inner fast moving eddies rather than with outer, large slow moving eddies. Experimental studies conducted by Brown et. al.[10] on counterflow flames experiencing an oscillating strain rate indicated that the extinction strain rate for unsteady counterflow flames exceeded the critical steady-state strain rate, and that the unsteady flame chemistry lagged aerodynamic oscillations by a time equivalent to the advective time scale.

The role of buoyancy-induced instability in nonpremixed flames has been investigated in previous experimental[11] and computational studies[12,13]. The instability leads to the flame flickering phenomena, whereby the nonpremixed flame is periodically pinched by convecting vortices, causing large-scale, low-frequency oscillation in the flame surface. Shaddix and Smyth[14] focused on identifying the mechanisms responsible for the enhanced sooting behavior of strongly flickering jet diffusion flames. Other studies have examined the interaction of a single vortex with a premixed flame, focusing on how each eddy wrinkles the flame and how the flame alters the eddy. Roberts and Driscoll[15] studied a single toroidal vortex in a premixed laminar flame, and found that weak vortices were completely attenuated primarily due to volume expansion. Strong vortices did survive flame passage, but only if they could weaken the flame due to stretch effects. Keller et. al.[16] showed that the inlet jet formed a strong toroidal

vortex, which was responsible for the convection and mixing of the reactants with the residual hot products, preparing them for a rapid, almost volumetric, combustion process.

In summary, although oscillating flames and flame-vortex interactions have been studied extensively, previous investigations have generally examined these phenomena in the context of either nonpremixed or premixed flames, but not with respect to a partially premixed flame (PPF) containing both premixed and nonpremixed reaction zones. Compared to either a premixed flame or a nonpremixed flame, the response of a PPF to perturbations or to a vortex may be significantly different due to thermochemical and transport interactions between the two reaction zones. This provided the major motivation for the present study. In addition, while the state relationships are fairly well established for nonpremixed flames, they have been introduced for partially premixed flames only recently. Consequently, another motivation for the present study was to investigate the existence of state relationships for unsteady partially premixed flames.

The present investigation has two major objectives. The first is to examine the effects of coflow on the structure and stability of normal- and zero-gravity partially premixed flames established on a Wolfhard-Parker slot burner, which is a geometry that we have used extensively to characterize PPFs[7,17,18]. Here the flame response to inherent and forced perturbations and the associated flame-vortex interactions are also investigated. The second objective is to examine the structure of unsteady partially premixed flames. In particular, the investigation focuses on interactions between the two reaction zones and the existence of state relationships for oscillating partially premixed flames. Our previous studies have focused on these aspects in steady flames.

2.0 Mathematical Model

The simulations are based on the direct numerical solution of the time-dependent, two-dimensional governing equations for a reacting flow. Using a Cartesian (x, y) coordinate system, the equations can be written in a generalized form as:

$$\frac{\partial(\rho\phi)}{\partial t}+\frac{\partial(\rho u\phi)}{\partial x}+\frac{\partial(\rho v\phi)}{\partial y}=\frac{\partial}{\partial x}\left(\Gamma^{\phi}\frac{\partial\phi}{\partial x}\right)+\frac{\partial}{\partial y}\left(\Gamma^{\phi}\frac{\partial\phi}{\partial y}\right)+S^{\phi} \qquad (1)$$

Here ρ denotes density, and u and v denote the transverse (x) and axial (y) velocity components, respectively. The general form of Eq. (1) represents the mass, momentum, species, or energy conservation equations depending on the variable used for ϕ. The transport coefficients Γ^{ϕ} and the source term S^{ϕ} appearing in the governing equations are provided in our previous publication[6]. A body force term due to gravitational field is included in the axial momentum equation. The set of equations given by Eq. (1) is completed using the global-species conservation equation

$$Y_{N_s}=1.0-\sum_{1}^{N_s-1}Y_i \qquad (2)$$

and the state equation

$$p=\rho T R_0\sum_{1}^{N_s}\left(\frac{Y_i}{M_i}\right) \qquad (3)$$

where R_0 denotes the universal gas constant, T the temperature, Y_i the mass fraction of species I, M_i and molecular weight, and N_s the total number of species.

The solution of the governing equations (1)-(3) requires information on the thermodynamic and transport properties. These properties are considered to be temperature- and species-dependent. The algorithm used to compute them is based on Chapman-Enskog collision theory, Lennard-Jones potentials, and the Wilke semi-empirical formulae. The

enthalpy and specific heat for each species are calculated using the polynomial curve fits compiled by Burcat[19]. The secondary diffusion effects and thermal radiation are neglected in the present study.

The methane-air chemistry is modeled by employing a detailed reaction mechanism due to Peters[20] that considers 81 elementary reactions and 24 species (N_s = 24); namely CH_4, O_2, CH_3, CH_2, CH, CH_2O, CHO, CO_2, CO, H_2, H, O, OH, H_2O, HO_2, H_2O_2, C_2H, C_2H_2, C_2H_3, C_2H_4, C_2H_5, C_2H_6, CHCO, and N_2. Nitrogen is assumed to be an inert species in our simulations.

2.1 The Numerical Solution

The numerical solution of the governing equations is based on the algorithm developed by Katta et al.[21]. It employs a finite volume approach with a staggered, non-uniform grid system. Grid lines are clustered near the shear layer and the reaction zones to resolve the steep gradients of the dependent variables in these regions. The finite-difference forms of the momentum equations are obtained using implicit QUICKEST (Quadratic Upstream Interpolation for Convective Kinematics with Estimated Streaming Terms) scheme[22] that is third-order accurate in both space and time, while those of the species and energy equations are obtained using a hybrid scheme of Spalding[23]. An iterative ADI (Alternating Direction Implicit) technique is utilized for solving the resulting (N_s+3) system of algebraic equations.

The computational domain is bounded by the symmetry plane and an outflow boundary in the transverse direction, and by the inflow and another outflow boundary in the axial direction. Both the computational domain and the boundary conditions are depicted in Fig. 1. Symmetric conditions are applied at the left boundary, whereas the right boundary is treated as a free surface. At the inflow boundary, except for the wall where no–slip boundary conditions are imposed, uniform velocity profiles are assumed for both the inner fuel–rich and outer fuel–

lean streams. The temperature and species mass fraction profiles are also assumed to be uniform at the inflow boundary. The flow variables at the outflow boundary (at the top) are obtained using an extrapolation procedure with weighted zero and first–order terms. The main criterion used in selecting the weighting functions is that the flow should exit the outflow boundary without being distorted. In addition, the outflow boundaries in both directions are located sufficiently far from the respective inflow and symmetric boundaries to minimize the propagation of disturbances from the boundaries into the region of interest.

Numerical simulations are performed using a non-uniform 121×61 grid system in a 100mm × 150mm computational domain. The grid-independence of the numerical solution has been discussed by Katta et al.[21] and Azzoni[24]. Additional results concerning grid independence in the present study for both the 0- and 1-g flames have been reported by Shu[25]. The entire computational domain is initialized with the condition prescribed at the inflow boundary. The flow field obtained with steady-state calculations is employed as the initial condition for the unsteady simulations.

The species and energy conservation equations are first solved simultaneously to obtain the species mass fractions and the temperature. A stable numerical integration procedure is achieved by coupling the species and energy equations through the source terms. The momentum and the mass continuity equations are then solved to complete the calculations. At every time step, the pressure field is calculated by solving the pressure Poisson equations simultaneously and utilizing the LU matrix decomposition technique.

3.0 Results and Discussion

A schematic diagram of the Wolfhard-Parker slot burner used to establish the two-dimensional partially premixed methane-air flames is shown in Fig. 1. A rich fuel-air mixture

is introduced from the central (inner) slot, and air from the two outer slots. The central fuel slot is 7.5 mm wide and 42 mm long (aspect ratio of 5.6), and the outer air slots are each 15 mm wide and 42 mm long. As depicted in Fig.1, the computational model considers only the right half of the burner.

3.1 Validation: Comparison with Measurements for Steady Flames

The computational model was validated by comparing its predictions with the nonintrusive measurements for steady partially premixed flames (PPFs). Figure 2 presents a comparison of the predicted heat release rates with the experimentally-obtained excited C_2^*-chemiluminescent images of three PPFs established at equivalence ratios ϕ = 1.5, 1.7 and 2.0 respectively. The velocities in both the incoming fuel (V_{reac}) and air streams (V_{air}) are 30 cm s^{-1}. The chemiluminescence images were obtained using a 513×480 pixel intensified and gated solid–state camera (ITT F4577). In an earlier investigation[5], we have described this measurement technique in more detail, and also established a direct correlation between the C_2^*-chemiluminescence signal and the heat release rates.

Both the C_2^*–signal and the predicted heat release depict two reaction zones, one an inner premixed reaction zone and the other an outer nonpremixed reaction zone. For the three cases depicted in Fig. 2, the simulation and experiment show excellent agreement with respect to the spatial location of the reaction zones. The region near the apex of the nonpremixed reaction zone has a weaker chemiluminescent intensity than the predictions indicate. This is due to the fact that C_2^* radicals are nearly nonexistent in this region.

As ϕ is increased, both the inner and outer reaction zone heights increase. Since the global residence time is held constant in the three cases, the variation of the inner reaction zone height occurs due to the effect of ϕ on the chemical reaction time. Since the chemical time

increases as ϕ is increased, the inner premixed reaction zone moves to increasingly higher axial locations. The outer nonpremixed reaction zone height adjusts to that of the inner premixed zone, since the outer reaction establishes itself at locations where stoichiometric mixing conditions exist. As discussed by Shu et al.[5], the chemistry in this zone is characterized by the oxidation of the "intermediate fuels", CO and H_2, which are transported from the inner premixed reaction zone. Thus, the stoichiometry in the nonpremixed reaction zone is defined with respect to CO and H_2.

As the level of partial premixing is reduced, i.e., ϕ is increased, both the chemiluminescent signal and the simulated heat release rates decrease along the sides of the inner reaction zone, with higher levels being associated with the flame tip and base. Therefore, it appears that the reaction is more vigorous at the tip and base of the inner reaction zone than along its sides. The heat release rate progressively decreases along the outer nonpremixed region at downstream locations as the oxidation of CO and H_2 is completed. The nonpremixed reaction region has a weak tip, with reaction rates being stronger in upstream region of that flame.

In summary, there is excellent agreement between the predictions and measurements in terms of the reaction zone topography. More quantitative validations of the computational model in terms of velocity, temperature, and major species mole fractions have been provided in our earlier investigations on steady partially premixed flames[5,7,24,26].

3.2 Comparison of 1-g and 0-g Flame Structures

Figure 3 depicts the flame structures in terms of heat release rates and velocity vectors for 0– and 1-g partially premixed flames established at $\phi = 2.0$, $V_{reac} = 30$ cm s^{-1}, and without any coflow. Except for the absence of gravity in the 0-g flame, both flames are established

under identical conditions. The flame structure is generally determined by the combined effects of thermochemistry, advection and diffusive transport. Under 1-g conditions, the flame heat release produces both flow dilatation and buoyant convection. Flow dilatation or gas expansion due to the heating causes downstream motion normal to the flamefront, which is quite evident in the region downstream of the inner premixed reaction zone for both 1- and 0-g flames. The buoyant gases accelerate the flow in an opposite direction to the gravity vector, causing air entrainment that enhances the fuel–air mixing and, consequently, influences the upstream region. The effect of flow dilatation is to push the outer nonpremixed reaction zone away from the central plane, while the buoyant convection has the opposite effect. For the 1-g flame, in the absence of coflow, the latter effect dominates. Consequently, the outer nonpremixed reaction zones differ distinctly for the 0- and 1-g flames. For the latter, this reaction zone is more compact and closer to the inner premixed reaction zone, and has a closed tip. Thus, the effect of gravity on a partially premixed flame is to reduce the spatial separation, and, thereby, enhance interactions between the two reaction zones. An evidence of the enhanced interaction between the two reaction zones is that the height of the inner premixed zone is reduced for the 1-g flame.

Another prominent effect of buoyant acceleration is to induce a well–organized, periodic oscillation or flickering of the outer nonpremixed reaction zone of the 1-g flame. The flame flicker, whereby the flame is periodically pinched by a convecting vortex generated by an buoyancy–induced instability, has been examined in previous experimental and computational studies; see for example, Yuan et al.[11], Davis et al.[12] and Ellzey & Oran[13]. However, these studies have discussed this phenomena in the context of either nonpremixed or premixed flames, but not with respect to a partially–premixed flame. In Fig. 3, the presence of a vortex outside the nonpremixed reaction zone is evident from the velocity vectors. In addition, the

interaction of this vortex with the outer reaction zone, whereby the vortex is compressing the lower part of the zone and stretching the upper part, can be observed from the heat release rate contours and velocity vectors. The transient flame structure associated with the buoyancy-induced instability is further discussed further in later sections.

3.4 Effect of Coflow Velocity on Flame Structure

Since the PPF structure is strongly influenced by the entrainment caused by buoyant acceleration, it is of interest to examine how the entrainment and the flame structure are affected by coflow. The effect of coflow velocity (V_{air}) on the global structure of 0- and 1-g partially premixed flames is illustrated in Figs. 3 and 4. In each figure, the flame structure is depicted in terms of the heat release rates and velocity vectors.

For 0-g flames, as the magnitude of V_{air} is increased, the advection in the nonpremixed region is enhanced, which moves the outer nonpremixed zone closer to the centerline. Consequently, the spatial separation between the two reaction zones decreases, leading to enhanced interaction between them. Thus at higher coflow velocities, the global structure of 0-g flame becomes similar to that of 1-g flame. However, for the cases depicted in Figs. 3 and 4, the 0-g flames exhibit a stable behavior. In contrast, the corresponding 1-g flames exhibit well-organized oscillations for low coflow velocities, but stable behavior for high coflow velocities. Consequently, two distinct regimes can be identified to characterize the effects of coflow and gravity on partially premixed flames. These two regimes are defined in terms of the velocity ratio $V_R = V_{air}/V_{react}$. Previous studies dealing with buoyant jets[28] have delineated these regimes in terms of buoyancy-dominated and inertia-dominated regimes. Similar arguments are not applicable in the present study dealing with buoyant partially premixed flames, since flames involve thermal expansion due to heat release as well as a significant increase in viscosity due

to high temperatures. Moreover, in the present study, the two regimes are defined by varying the coflow velocity, while in the cited work, the jet velocity was varied.

In the low coflow velocity regime ($V_R \leq 1$), the flame structure, especially in the outer nonpremixed reaction zone, of both 0- and 1-g flames is strongly sensitive to the changes in V_R. In contrast, in the high coflow velocity regime ($V_R > 1$), the global structures of 0- and 1-g flames become relatively insensitive to the coflow velocity. In addition, structural differences between the 0- and 1-g flames are quite pronounced in the first regime, but become insignificant in the second regime. For example, at low coflow velocities, the spatial separation between the inner and outer reaction zones is much larger for the 0-g flame compared to that for the 1-g flame. Consequently, as indicated in Figs. 3 and 4, the outer reaction zone of the 1-g flame is relatively more compact, taller, and closer to the inner reaction zone. In addition, the outer reaction zone of the 1-g flame generally has a closed tip, while that of the 0-g flame has an open tip.

A more significant difference between the 0- and 1-g flames in the low coflow velocity regime is the presence of flame flickering that is characterized by the well-organized oscillations in both the inner and outer reaction zones of the 1-g flame. The oscillation amplitude is much higher in the outer reaction zone compared to that in the inner reaction zone. The flame oscillations in the case of 1-g flame become progressively less pronounced as the coflow velocity is increased, and the flame becomes steady in the high coflow velocity regime. In contrast, the 0-g flame exhibits steady behavior in both the low and high coflow velocity regimes. In Table 1, we summarize the response of the 0- and 1-g flames to variations in the coflow velocity in both regimes.

The amplitude and frequency of oscillations can be obtained by recording the temperature history at a fixed spatial location. Figure 5 presents these temperature history plots

for the three 1–g flames depicted in Fig. 4. The amplitude and frequency obtained from the temperature history are provided in Table 2. As the coflow velocity is reduced, the flickering amplitude increases, and the flickering frequency decreases. The effect of coflow is, however, much stronger on the amplitude compared to that on frequency. The variation of flickering amplitude with V_R implies that the buoyancy-induced instability can be controlled by varying the ratio of coflow velocity to inner jet velocity. This result is consistent with those of previous experimental and numerical investigations dealing with nonpremixed flames[12,21,29] and partially-premixed triple flames[24] at normal gravity. As indicated in these investigations, increasing the coflow velocity decreases the vortex size and the oscillation amplitude. The variation of flickering frequency with V_R obtained from our simulations is also in accord with the previous experimental results on buoyant jet diffusion flames[29] and 1-g triple flames[24].

3.5 Transient Flame Behavior

The transient phenomena associated with flame flicker for the 1-g flame is depicted in Fig. 6, which present Instantaneous images in terms of the predicted heat release rates and velocity vectors during one oscillation period. The large-amplitude oscillation of the outer nonpremixed reaction zone caused by the buoyancy-induced convecting vortex is quite evident. As the vortex convects downstream, it produces both convex and concave curvature in the nonpremixed reaction zone. In addition, the upper part of this zone is pulled up or stretched in the transverse direction, and eventually pinched off by the vortex, leading to flame flicker. Due to a strong coupling between the two reaction zones, the large-amplitude oscillation in the outer reaction zone also induces an oscillation in the inner premixed reaction zone. Therefore, every location of the spatially evolving flow field experiences this self-excited oscillation. However, the amplitude of oscillation in the premixed zone is much smaller than that in the nonpremixed zone, indicating that the premixed zone exhibits significantly improved stability characteristics.

A more quantitative analog of the results presented in Fig. 6 is contained in Fig. 7. The mass fraction of the major species is averaged in the transverse direction, and this averaged mass fraction is plotted along the streamwise direction at different times during an oscillation period. These plots can be used to describe the global unsteady flame structure. As indicated in Figs. 7a and 7b, methane and oxygen are rapidly consumed near the burner exit ($Y \leq 21$ mm). This upstream region contains the entire inner premixed reaction zone and a part of the outer nonpremixed reaction zone (cf. Fig. 6), while the region downstream of $Y > 21$ mm only contains the outer nonpremixed reaction zone.

Methane is almost completely consumed in the upstream region, with a small remaining amount being consumed in the downstream region (nonpremixed zone) where additional oxygen is supplied by the coflowing air. Intermediate fuels (CO and H_2) are produced in the upstream region through partial oxidation of the fuel, and then consumed in the downstream region. The major combustion products (CO_2 and H_2O) are formed in both the upstream and downstream regions. The reactions involving the formation of H_2O proceed at a faster rate compared with those associated with CO_2 formation. The species profiles in Fig. 7 also indicate that the outer nonpremixed zone is subjected to a large-amplitude oscillation, whereas the oscillation amplitude in the inner premixed zone is relatively small.

3.6 State Relationships for Unsteady Partially Premixed Flames

The flamelet model of nonpremixed turbulent combustion has been analyzed in terms of a conserved scalar defined by the mixture fraction[30]. Since partially premixed flames contain regions of both premixed and nonpremixed combustion, a modified mixture fraction has been employed to examine the flamelet model for partially premixed turbulent combustion[31,32]. We have employed the conserved scalar approach based on a modified mixture fraction in

characterizing state relationships for steady partially premixed flames[17] and for examining the similitude between partially premixed flames in different configurations[4]. Here we employ a similar approach to examine the existence of state relationships for unsteady partially premixed flames. We define the modified mixture fraction in terms of elemental nitrogen mass fraction as

$$\xi = (Z_{N,\,max} - Z_N)/(Z_{N,\,max} - Z_{N,\,min}) \qquad (7)$$

where $Z_{N,\,max}$ denotes the elemental nitrogen mass fraction in the fuel stream, Z_N the local mass fraction of elemental nitrogen, and $Z_{N,\,min}$ the corresponding mass fraction in the air stream. Other elemental mass fractions or a combination of them, as proposed by Bilger[35] can also be used to examine the state relationships.

Figure 8 presents the modified mixture fraction (left) and heat release rate (right) contours for the 1– and 0–g flames established at $\phi = 2.0$, $V_{reac} = 30$ cm s^{-1}, and $V_{air} = 0$. As noted earlier, the 0-g flame for these conditions is steady, while the corresponding 1-g flame is unsteady. Therefore, the contour plots for the latter are shown at two different times during a single oscillation period. In spite of differences in the contour shapes, both the modified mixture fraction and heat release rate contours are effective in identifying the two reaction zones, and suggest that the thermochemistry and state relationships are well–correlated. In terms of the ξ-contours, the rich premixed reaction zone for both 1- and 0-g flames lies between $0.72 < \xi < 0.8$, and the nonpremixed zone between $0.47 < \xi < 0.55$. It is interesting to note that the inner and outer reaction zones of the 1– and 0–g flames are represented approximately by the same ξ–contours, even though these flames exhibit significantly different structures in the physical space. This suggest that the conserved scalar approach based on a

modified mixture fraction is effective in characterizing state relationships for these unsteady partially premixed flames.

Figure 9 presents state relationships for the temperature and major species mole fractions with respect to ξ for the 0– and 1–g flames at two axial locations above the burner exit. The species include the major reactant species (CH_4 and O_2), the intermediate fuel species (CO and H_2), and the major product species (CO_2 and H_2O). In order to identify the locations of the two reaction zones, the corresponding heat release rate profiles are also shown in Fig. 9a. Since the 1-g flame for these conditions is unsteady, the profiles for this flame are shown at four different times during one oscillation period. The profiles at the lower axial location (i.e., at 14–mm above the burner exit) depict both the reaction zones. The axial location of 30 mm lies above the premixed reaction zone and the profiles only cross the nonpremixed reaction zone. Although the 1- and 0-g flames have markedly different spatio-temporal characteristics, the temperature and major species profiles follow similar state relationships in terms of the modified mixture fraction for the two flames. Thus, an important observation from these results is that the modified mixture fraction is effective in characterizing the structure of both steady and unsteady partially premixed flames**.**

The species mole fraction profiles with respect to the modified mixture fraction provide useful insight about the flame structure, especially regarding scalar transport and interactions between the two reaction zones. For instance, the CH_4 profiles indicate that methane is mostly consumed in the inner premixed zone, while those of CO and H_2 indicate that these (intermediate fuel) species are produced in the premixed reaction zone and then transported to and consumed in the nonpremixed reaction zone. The main consumption reaction for these two species are $H_2 + OH \Leftrightarrow H_2O + H$, and $CO + OH \Leftrightarrow CO_2 + H$. As indicated in Fig. 10, peaks in the H and OH radical concentration profiles also occur in the nonpremixed zone ($0.47 < \xi <$

0.55). This is further confirmed by the CO_2 and H_2O profiles, which have maximum concentrations in the nonpremixed reaction zone, implying that these species are mostly produced in this zone. Consequently, the nonpremixed zone has the highest temperature due to CO and H_2 oxidation (cf. Fig. 9a), and provides heat to the premixed zone.

In Fig. 10, we present state relationships for the three radical species (OH, H, and HO_2) mole fractions with respect to ξ for the 0– and 1–g flames at two axial locations. The minor species profiles also exhibit remarkable similarity for the two flames in the modified mixture fraction space, even though these flames have different structures in the physical and temporal spaces. In addition, the profiles provide insight regarding scalar transport and interactions between the two reaction zones. The maxima in the OH and H radical concentrations occur in the nonpremixed reaction zone. This implies that the nonpremixed zone represents a region of higher chemical activity from which H–atoms and OH radicals are transported to the premixed reaction zone. HO_2 radicals are produced through the reaction $H + O_2 + M \Leftrightarrow HO_2 + M$ and mainly consumed through the reaction $HO_2 + H \Leftrightarrow OH + OH$ both in the premixed and nonpremixed reaction zones. This is confirmed by the HO_2 profiles presented in Fig. 10b along with the O_2 profiles presented in Fig. 9. These profiles also indicate that the chemical activity involving HO_2 is much higher in the premixed zone compared to that in the nonpremixed zone, and the production of HO_2 occurs upstream of the premixed reaction zone ($\xi > 0.9$), and outside of the nonpremixed reaction zone ($\xi < 0.3$).

In order to examine the applicability of the mixture fraction approach for different coflow velocities, in Fig. 11 we present the temperature profiles with respect to ξ for the 0– and 1–g flames established at two other conditions. The two reaction zones are again identified by superimposing the heat release rate profiles. Although the heat release rate profiles indicate

scatter, the temperature profiles again confirm the effectiveness of the mixture fraction approach in characterizing state relationships for steady and unsteady partially premixed flames over a wide range of conditions. This has important implications for the modeling of partially premixed turbulent combustion, since we observe that it is possible to develop laminar flamelet libraries for both steady and unsteady partially premixed flames based on the mixture fraction approach.

4. Conclusions

We have presented a numerical investigation of the structure of steady and unsteady methane-air partially premixed flames (PPF) established on a Wolfhard-Parker slot burner under zero- and normal-gravity conditions. The numerical model was validated by establishing their grid independence, and comparing the predicted heat release rates with the experimentally obtained chemiluminescence emission for representative PPFs established at near-unity Froude number and three different levels of partial premixing. Simulations were then used to characterize the effect of gravity on the flame structure and interactions between the reaction zones, investigate the effect of coflow on the structure and stability of 1-g and 0-g flames, and determine the existence of state relationships in terms of a modified mixture fraction for unsteady partially premixed flames**.**

For both 0- and 1-g PPFs, combustion occurs in two reaction zones, namely a premixed zone and a nonpremixed zone. There were, however important 1 differences between the structures of 0- and 1-g flames. Due to the enhanced advection and entrainment caused by buoyancy, the nonpremixed reaction zone of the 1-g flame was more compact with a closed tip, and located closer to the premixed zone, which enhanced interactions between the two reaction zones. A more prominent effect of buoyant acceleration was to induce self-excited, periodic oscillations of the 1-g flame. The buoyancy-induced flow instability caused coherent vortex

structures to develop and interact with the outer nonpremixed reaction zone, causing periodic distortion and pinch-off (flicker) of this zone.

The effects of coflow velocity and gravity on partially premixed flames were characterized by a parameter V_R, defined as the ratio of the coflow velocity to the jet velocity. For $V_R \leq 1$ (low coflow velocity regime), the structures of both 0- and 1-g flames were strongly sensitive to changes in V_R, while they were only mildly affected by coflow velocity in the high coflow velocity regime ($V_R > 1$). In addition, structural differences between the 0- and 1-g flames were found to be pronounced in the first regime, but relatively insignificant in the second regime. A significant difference between the 0- and 1-g flames in the low coflow velocity regime was the presence of flow instability, which manifests itself in the self-excited oscillations of the 1-g flame and concomitant flickering of its nonpremixed reaction zone. For $V_R \leq 1$, as the coflow velocity was increased, the oscillation amplitude decreased while the frequency increased, in accordance with the previous experimental and computational investigations of 1-g jet diffusion flames. The oscillations became progressively less pronounced as the coflow velocity was increased, and eventually the 1-g flame became steady in the high coflow velocity regime. In contrast, the 0-g flame exhibited stable behavior in the entire coflow velocity regime.

The modified conserved scalar approach was found to be effective in characterizing the flame structure and developing state relationships for both steady and unsteady partially premixed flames. This was demonstrated by the fact that the temperature as well as the major and minor species profiles follow similar state relationships in terms of the modified mixture fraction for the 0- and 1-g flames, even though these flames have markedly different spatio-temporal characteristics. This has fundamental relevance to the modeling of analogous

turbulent flames that involve effects due to differential diffusion, flame curvature and spatio-temporally varying strain rates.

Acknowledgment

This research was partially funded by the NASA Office of Physical and Biological Sciences, Microgravity Science Division, Grant, No. NCC3–688. Results presented in this paper were computed by Dr. Z. Shu as part of his Ph.D. thesis. Many fruitful discussions with Prof. Ishwar K. Puri of Virginia Tech, and Dr. V. R. Katta of ISSI are greatly appreciated.

References

[1]I. Yamaoka, & H. Tsuji, "The Structure of Rich Fuel-Air Flames in the Forward Stagnation Region of a Porous Cylinder," *Proc. Combust. Inst*. **15**, 637 (1974).

[2]I. Yamaoka & H. Tsuji, "Structure Analysis of Rich Fuel-Air Flames in the Forward Stagnation Region of a Porous Cylinder," *Proc. Combust. Inst*. **16**, 1145 (1976).

[3]I. Yamaoka & H. Tsuji, "An Experimental Study of Flammability Limits Using Counterflow Flames," *Proc. Combust. Inst*. **17**, 843 (1978).

[4]S. K. Aggarwal & I., K. Puri, "Flame Structure Interactions and State Relationships in an Unsteady Partially Premixed Flame," *AIAA J*. **36**, 1190 (1998).

[5]Z. Shu, B. J. Krass, C. W. Choi, S. K. Aggarwal, V. R. Katta, & I. K. Puri, "An Experimental and Numerical Investigation of the Structure of Steady Two-Dimensional Partially-Premixed Methane-Air Flames," *Proc. Combust. Inst*. **27**, 625 (1998).

[6]Z. Shu, C. W. Choi, S. K. Aggarwal, V. R. Katta, & I. K. Puri, "Gravity Effects on Steady Two-Dimensional Partially-Premixed Methane-Air Flames," *Combust. Flame* **118**, 91 (1999).

[7]I. K. Puri, S. K. Aggarwal, S. Ratti & R. Azzoni, On the Similitude Between Lifted And Burner–Stabilized Triple Flames: A Numerical and Experimental Investigation," *Combust. Flame* **124**, 311 (2001).

[8]A. J. Yule, N. A. Chigier, S. Ralph, R. Boulderstone, & J. Ventura, "Combustion-Transition Interaction in a Jet Flame," *AIAA J.* **19**, 752 (1981).

[9]A. J. Yule, "Large Scale Structure in the Mixing Layer of a Round Jet," *J. Fluid Mech.* **89**, 413 (1978).

[10]T. M. Brown, R. W. Pitz, & C. J. Sung, "Oscillating Stretch Effects on the Structure and Extinction of Counterflow Diffusion Flames," *Proc. Combust. Inst*. **27,** 703 (1998).

[11]T. Yuan, D. Durox, & E. Villermaux, "An Analog Study for Flame Flickering," *Experiments in Fluids* **17**, 104 (1994).

[12]R. W. Davis, E. F. Moore, W. M. Roquemore, L. D. Chen, V. Vilimpoc, & L. P. Goss, "Preliminary Results of a Numerical-Experimental Study of the Dynamic Structure of a Buoyant Jet Diffusion Flame" *Combust. and Flame* **83**, 263 (1991).

[13]J. L. Ellzey & E. S. Oran, "Effects of Heat Release and Gravity on an Unsteady Diffusion Flame," *Proc. Combust. Inst*. **23**, 1635 (1990).

[14]R. C. Shaddix, & C. K. Smyth, "Laser-Induced Incandescence Measurements of Soot Production in Steady and Flickering Methane, Propane, and Ethylene Diffusion Flames," *Combust. Flame* **107**, 418 (1996).

[15]L. W. Roberts, & F. J. Driscoll, "A Laminar Vortex Interacting with a Premixed Flame: Measured Formation of Pockets of Reactants," *Combust. Flame* **87**, 245 (1991).

[16]O. J. Keller, K. P. Barr, & S. R. Gemmen, "Premixed Combustion in a Periodic Flow Field. Part I: Experimental Investigation," *Combust. Flame* **99**, 29 (1994).

[17]R. Azzoni, S. Ratti, I. K. Puri, & S. K. Aggarwal, "The Structure of Triple Flames Stabilized on a Slot Burner," *Combust. Flame* **119**, 23 (1999).

[18]S. K. Aggarwal & I., K. Puri & X. Qin, "A Numerical and Experimental Investigation of "Inverse" Triple Flames," *Physics of Fluids* **13**, 265 (2001).

[19]A. Burcat, "Thermochemical Data for Combustion Calculations," *Combustion Chemistry,* Springer-Verlag, New York, 455 (1984).

[20]N. Peters, "Flame Calculations with Reduced Mechanisms-An Outline, In Reduced Kinetics Mechanisms for Applications in Combustion Systems," *Lecture Notes in Physics,* N. Peters and B. Rogg (Eds.), Springer-Verlag, **m15**, 3 (1993).

[21]V. R. Katta, L. P. Goss & W. M. Roquemore, "Numerical Investigations of Transitional H_2/N_2 Jet Diffusion Flames," *AIAA J.* **32**, 84 (1994).

[22]B. P. Leonard, "A Stable and Accurate Convective Modeling Procedure Based on Quadratic Upstream Interpolation," *Computational Methods in Applied Mechanics and Engineering* **19**, 59 (1979).

[23]D. B. Spalding, "A Novel Finite Difference Formulation for Different Expressions involving both First and Second Derivatives," *Int. J. Num. Methods in Engr.* **4**, 551 (1972).

[24]R. Azzoni, "A Numerical Investigation of Methane-Air Triple Flames," MS Thesis, University of Illinois at Chicago, 1999.

[25]Z. Shu, "Steady and Unsteady Structure of Partially-Premixed Methane-Air Flames," Ph.D. Thesis, University of Illinois at Chicago, 2001.

[26]X. Qin, X. Xiao, S. K. Aggarwal, & I. K. Puri, "Analysis of Errors in Holographic Temperature Measurements in Steady Two-Dimensional Partially Premixed Flames," *Applied Optics*, Submitted, 2001.

[27]R. Azzoni, S. Ratti, I. K. Puri, & S. K. Aggarwal, "Gravity Effects on Triple Flames: Flame Structure and Flow Instability," *Phys. Fluids* **11**, 3449 (1999).

[28]E. R. Subbarao, & B. J. Cantwell, B. J. *J. Fluid Mech*. **245**, 69 (1992).

[29]A. Lingens, K. Neemann, J., Meyer & M. Schreiber, "Instability of Diffusion Flames," *Proc. Combust. Inst*. **26**, 1053 (1996).

[30]N. Peters, "Partially Premixed Diffusion Flamelets in Non-premixed Turbulent Combustion," *Proc. Combust. Inst*. **20**, 353 (1984).

[31]B. Rogg, F. Behrendt, & J. Warnatz, "Turbulent Non-premixed Combustion in Partially Premixed Diffusion Flamelets with Detailed Chemistry," *Proc. Combust. Inst*. **21**, 1533 (1986).

[32]K. Seshadri, I. K. Puri, & N. Peters, "Experimental and Theoretical Investigation of Partially Premixed Diffusion Flames at Extinction," *Combust. Flame* **61**, 237 (1985).

[33]H. N. Najm, P. H. Paul, C. J. Mueller, & P. S. Wyckoff, "On the Adequacy of Certain Experimental Observables as Measurements of Flame Burning Rate," *Combust. Flame* **113**, 312 (1998).

[34]B. V. Bennett, C. S. McEnally, L. D. Pfefferle, M. D. Smooke, "Computational and experimental study of axisymmetric coflow partially premixed methane/air flames," *Combust. Flame* **123**, 522 (2000).

[35]R. W. Bilger, "The structure of turbulent nonpremixed flames," *Proc. Combust. Inst*. **22**: 475 (1988).

Table 1: Response of 0-g and 1-g partially premixed flames to variation in coflow velocity.

Regime	0-g Flame	1-g Flame
Low coflow regime	Strong sensitivity to coflow	Strong sensitivity to coflow
	Outer reaction zone strongly affected by coflow	Outer reaction zone strongly affected by coflow
	Stable Flame	Oscillating Flame
High coflow regime	weak sensitivity to coflow	weak sensitivity to coflow
	Stable flame	Stable Flame

Table 2: Effect of coflow velocity on flickering amplitude and frequency for 1-g partially premixed flames.

V_{air} (cm/s)	V_R	Amplitude (%)	Frequency (Hz)
100	3.33	Steady flame	Steady flame
30	1.0	1	20
10	0.33	38	12
0	0	54	10.5

LIST OF FIGURES:

10. State relationships in terms of OH, H, and HO_2 mole fraction profiles plotted versus the modified mixture fraction (ξ) for the 1- and 0-g flames established at conditions corresponding to those of Fig. 10.

11. State relationships for temperature plotted as a function of ξ for 1- and 0-g flames for (i) $V_{reac} = V_{air} = 30$ cm s^{-1} and (ii) $V_{reac} = 30$ cm s^{-1}, $V_{air} = 100$ cm s^{-1}.

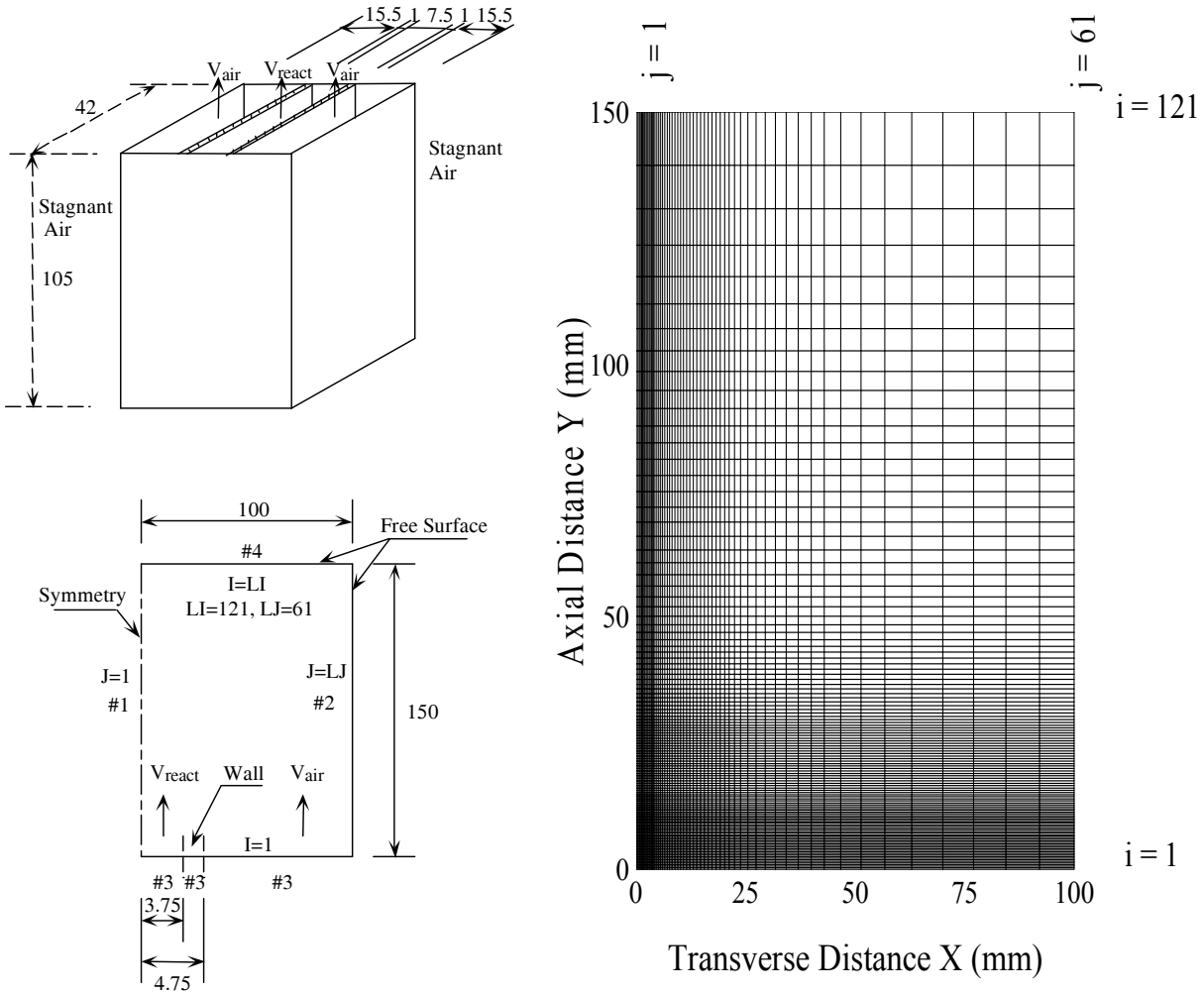
15.5 1 7.5 1 15.5
Vair Vreact Vair
42
Stagnant Air
Stagnant Air
105
100
Free Surface
#4
I=LI
LI=121, LJ=61
Symmetry
J=1
#1
J=LJ
#2
150
Vreact Wall Vair
I=1
#3 #3 #3
3.75
4.75
j = 1
j = 61
i = 121
i = 1
150
100
50
0
0 25 50 75 100
Axial Distance Y (mm)
Transverse Distance X (mm)

Figure 1

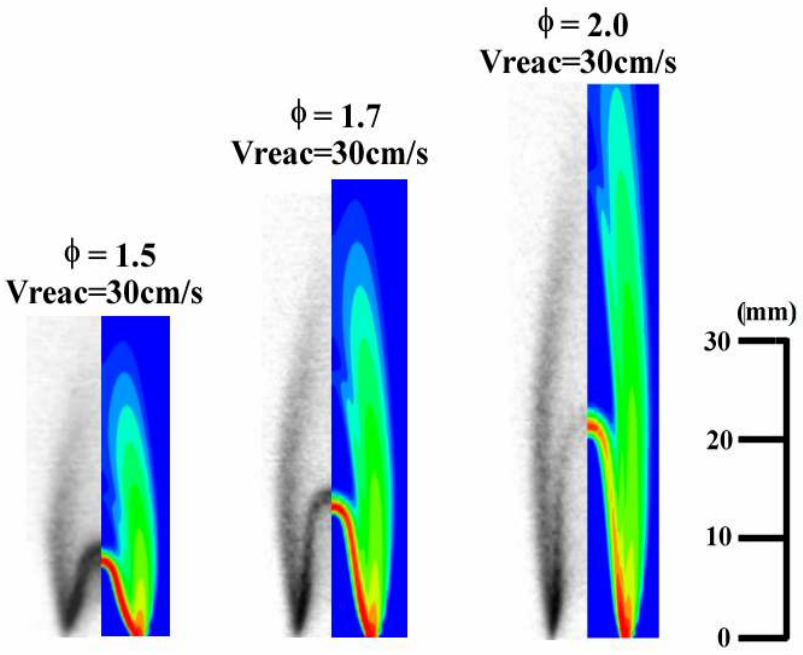

Figure 2

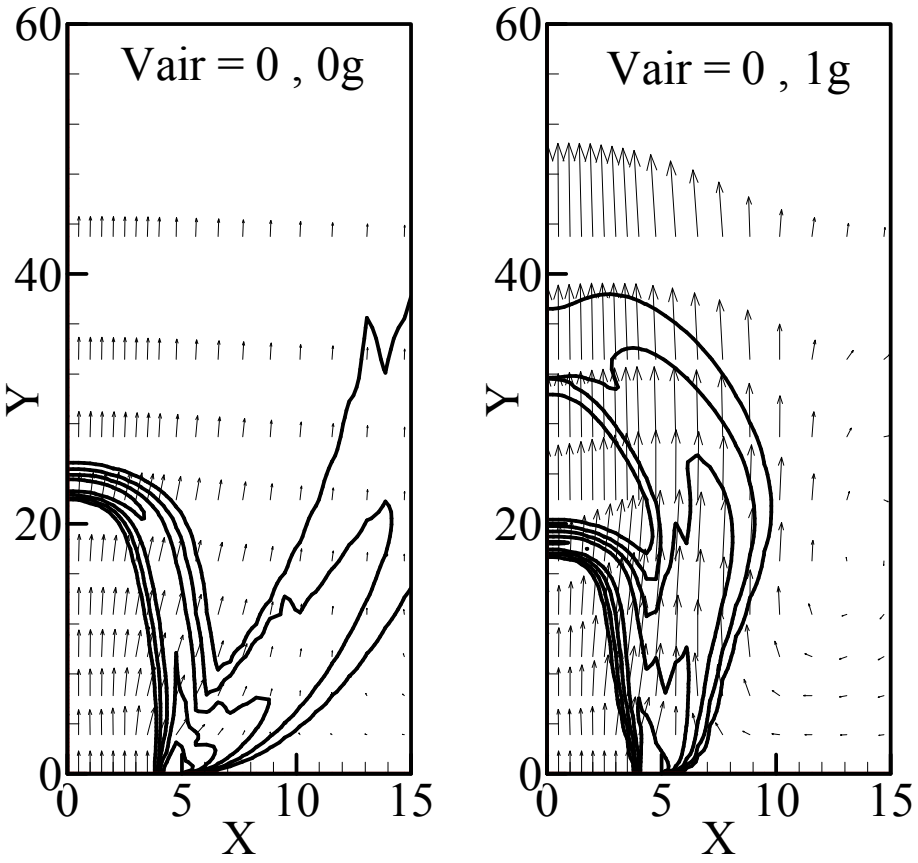

Figure 3

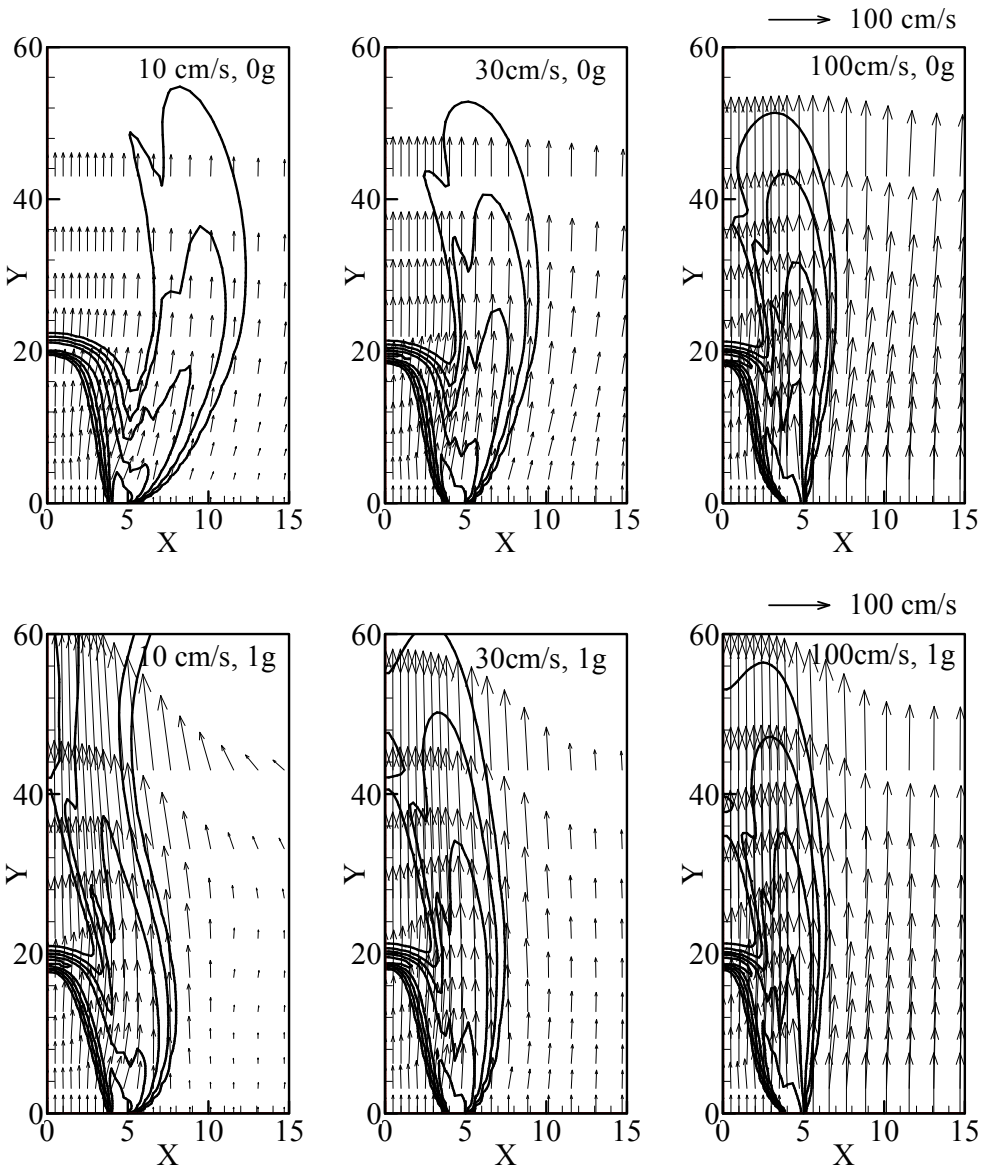
100 cm/s
10 cm/s, 0g
30cm/s, 0g
100cm/s, 0g
100 cm/s
10 cm/s, 1g
30cm/s, 1g
100cm/s, 1g
Y
X
0
20
40
60
0
5
10
15

Figure 4

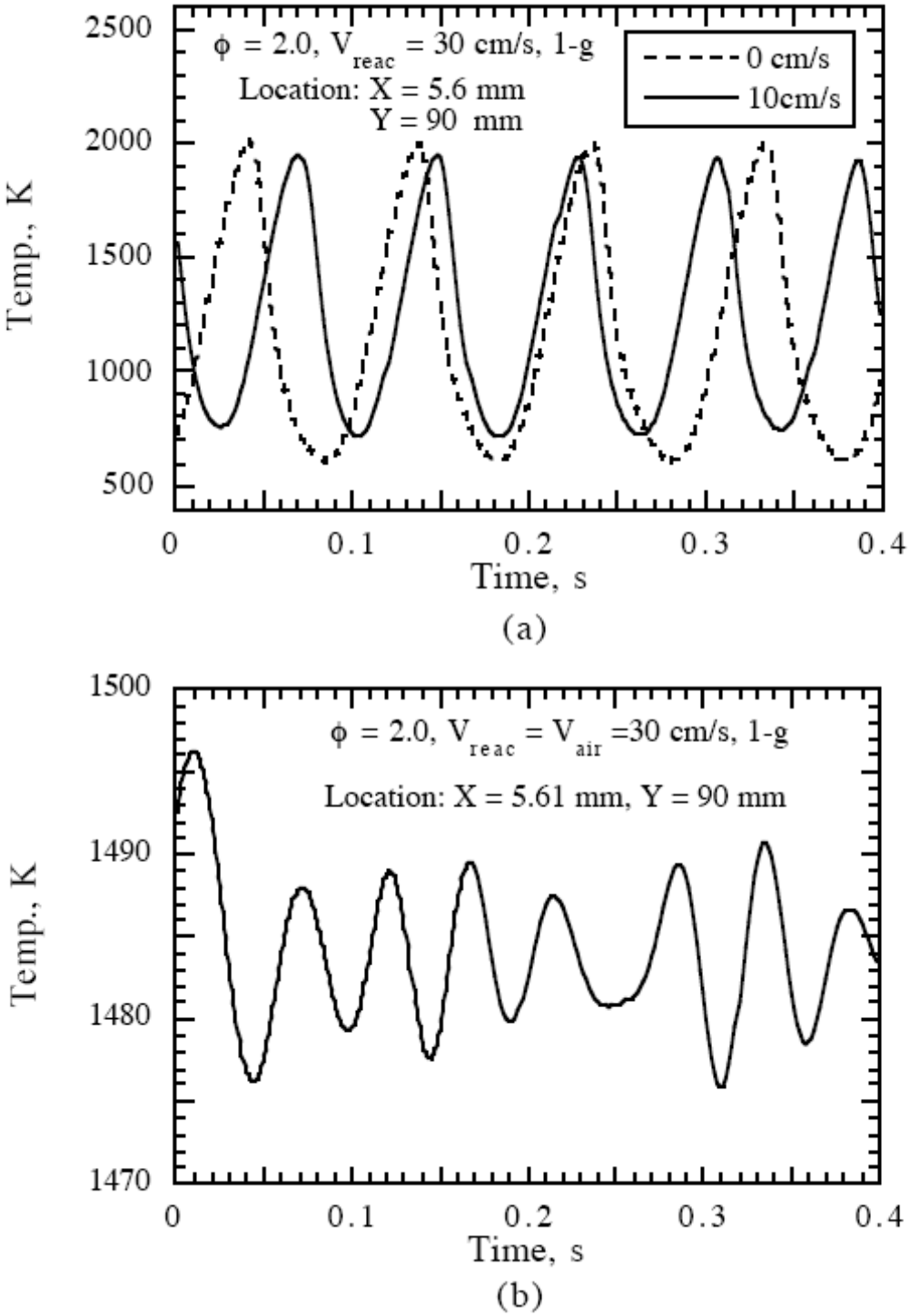
2500
2000
1500
1000
500
Temp., K
ϕ = 2.0, V reac = 30 cm/s, 1-g
Location: X = 5.6 mm
Y = 90 mm
0 cm/s
10cm/s
0
0.1
0.2
0.3
0.4
Time, s
(a)
1500
1490
1480
1470
Temp., K
ϕ = 2.0, V reac = V air =30 cm/s, 1-g
Location: X = 5.61 mm, Y = 90 mm
0
0.1
0.2
0.3
0.4
Time, s
(b)

Figure 5

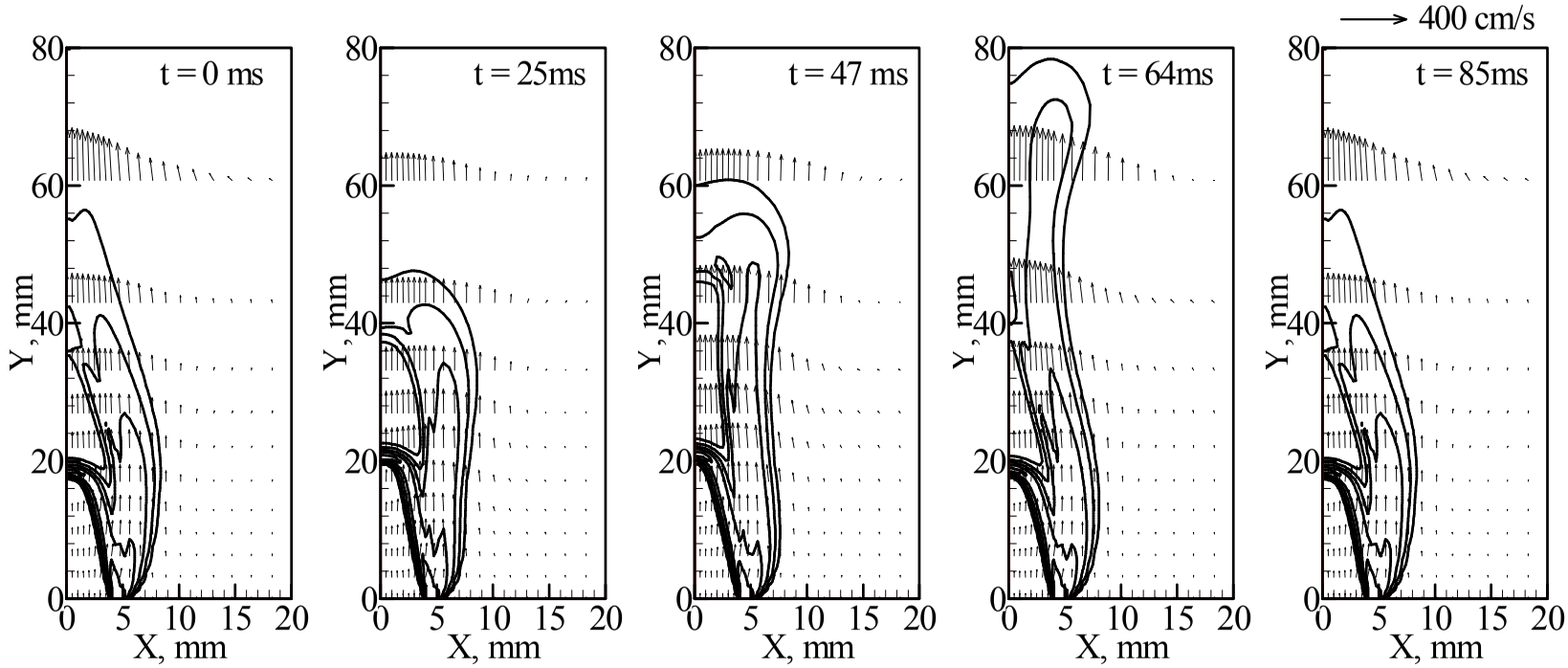
400 cm/s
t = 0 ms
t = 25ms
t = 47 ms
t = 64ms
t = 85ms
Y, mm
X, mm
0
20
40
60
80
0
5
10
15
20

Figure 6

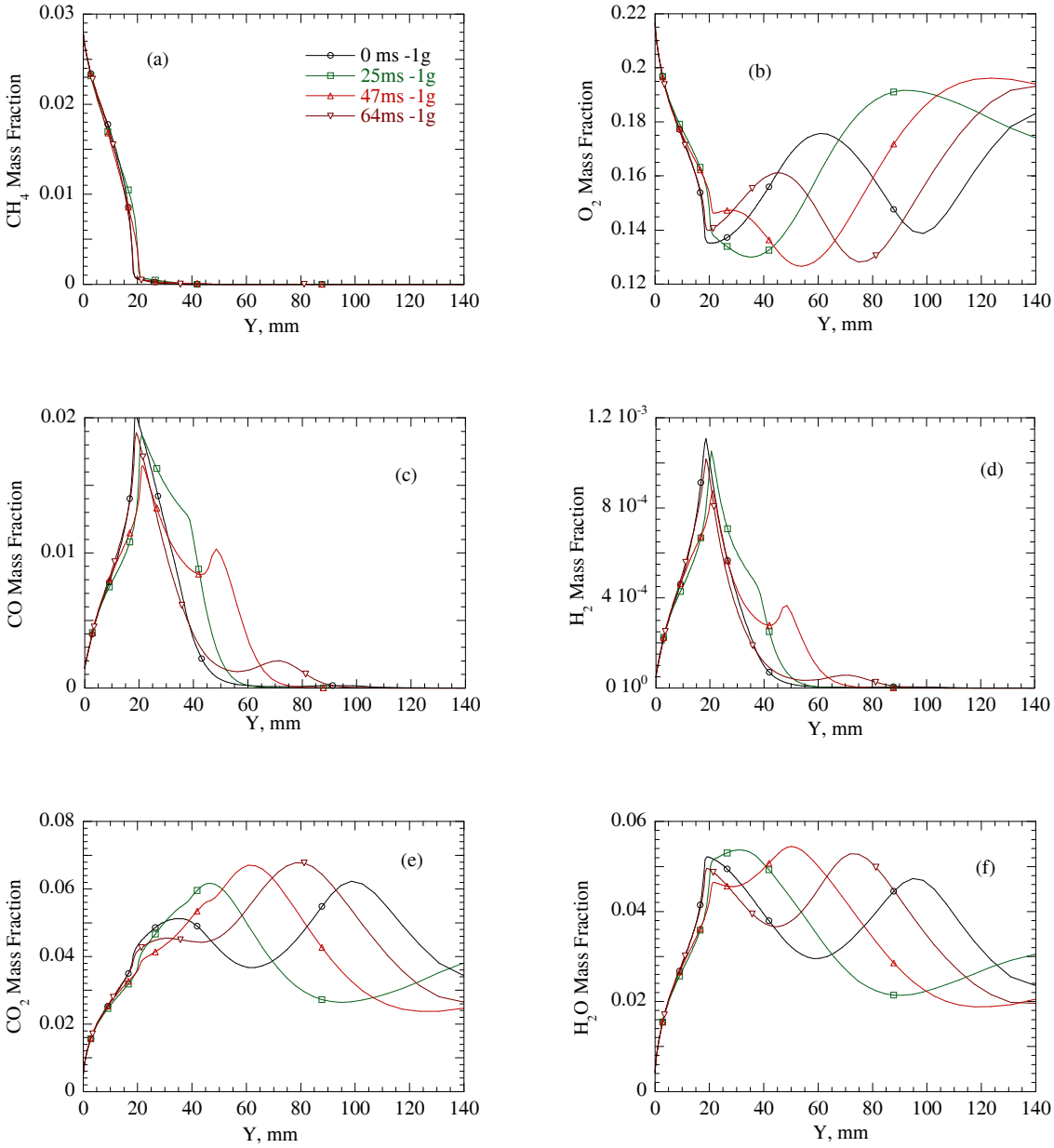
(a)
0 ms -1g
25ms -1g
47ms -1g
64ms -1g
CH4 Mass Fraction
Y, mm
(b)
O2 Mass Fraction
Y, mm
(c)
CO Mass Fraction
Y, mm
(d)
H2 Mass Fraction
Y, mm
(e)
CO2 Mass Fraction
Y, mm
(f)
H2O Mass Fraction
Y, mm

Figure 7

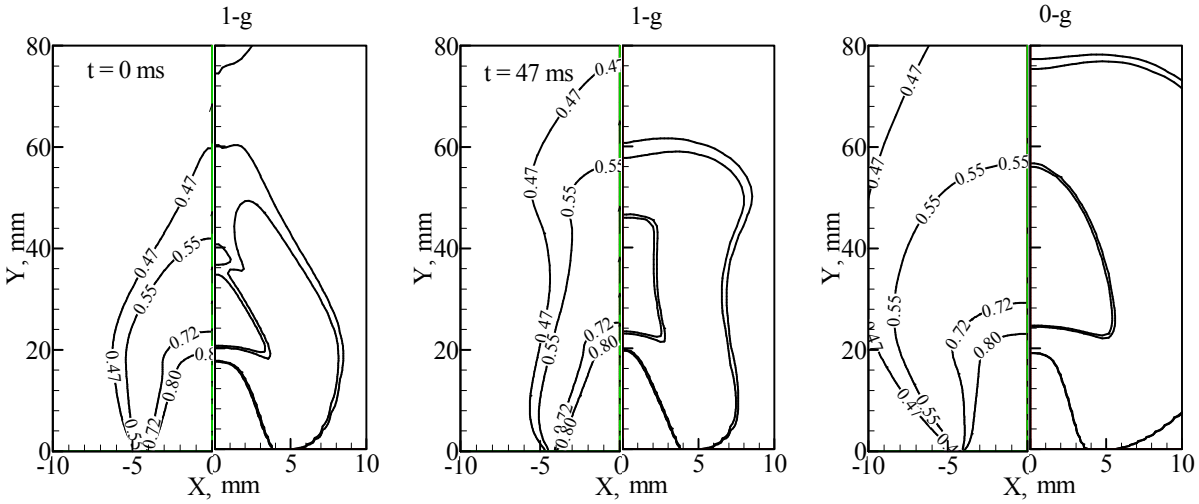

Phi = 2.0, Vreac = 30 cm/s and Vair = 10 cm/s

Figure 8

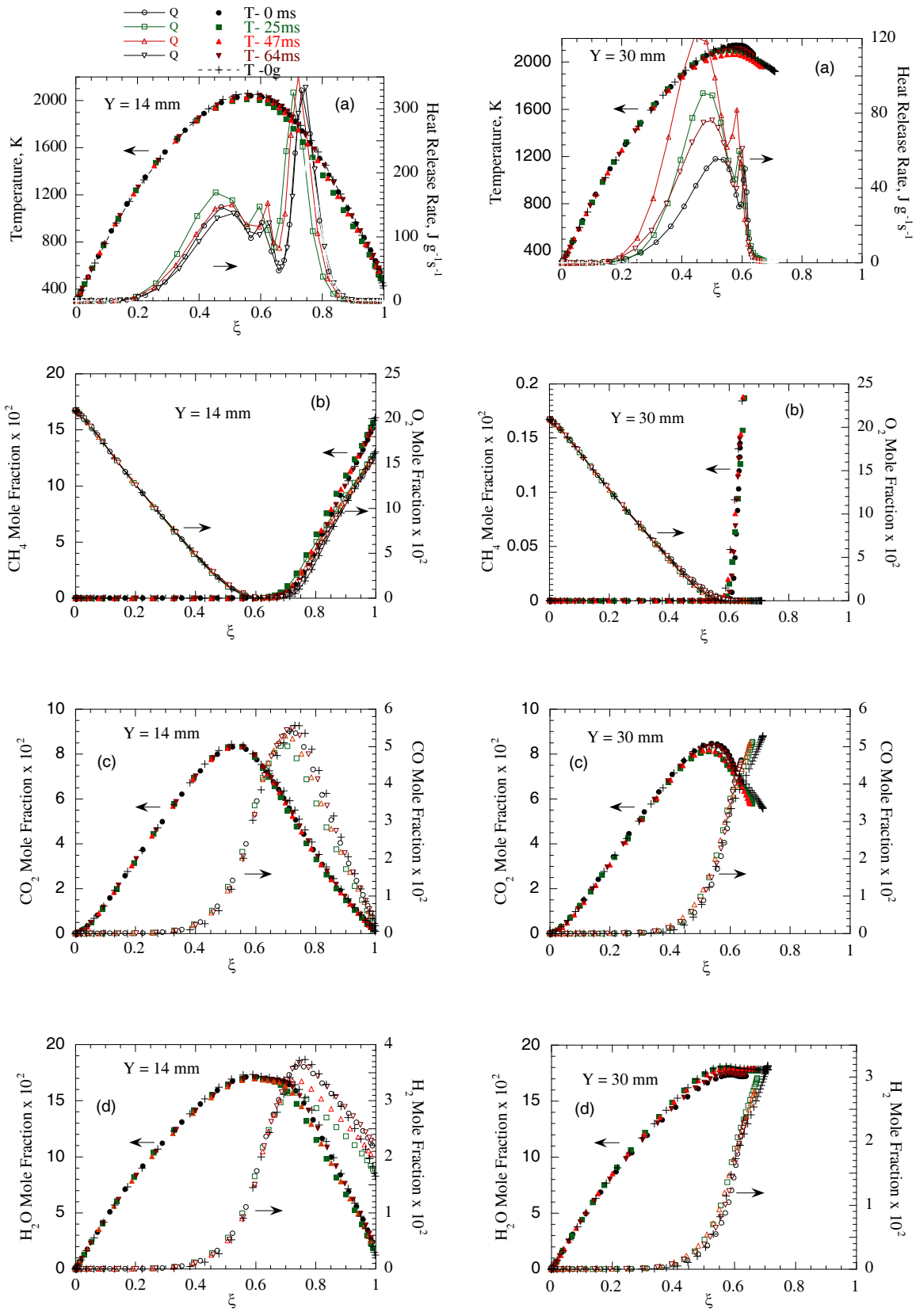
Q
Q
Q
Q
T- 0 ms
T- 25ms
T- 47ms
T- 64ms
T -0g
Y = 14 mm
(a)
Temperature, K
Heat Release Rate, J g-1s-1
ξ
Y = 30 mm
(a)
Temperature, K
Heat Release Rate, J g-1s-1
ξ
Y = 14 mm
(b)
CH4 Mole Fraction x 10^2
O2 Mole Fraction x 10^2
ξ
Y = 30 mm
(b)
CH4 Mole Fraction x 10^2
O2 Mole Fraction x 10^2
ξ
Y = 14 mm
(c)
CO2 Mole Fraction x 10^2
CO Mole Fraction x 10^2
ξ
Y = 30 mm
(c)
CO2 Mole Fraction x 10^2
CO Mole Fraction x 10^2
ξ
Y = 14 mm
(d)
H2O Mole Fraction x 10^2
H2 Mole Fraction x 10^2
ξ
Y = 30 mm
(d)
H2O Mole Fraction x 10^2
H2 Mole Fraction x 10^2
ξ

Figure 9

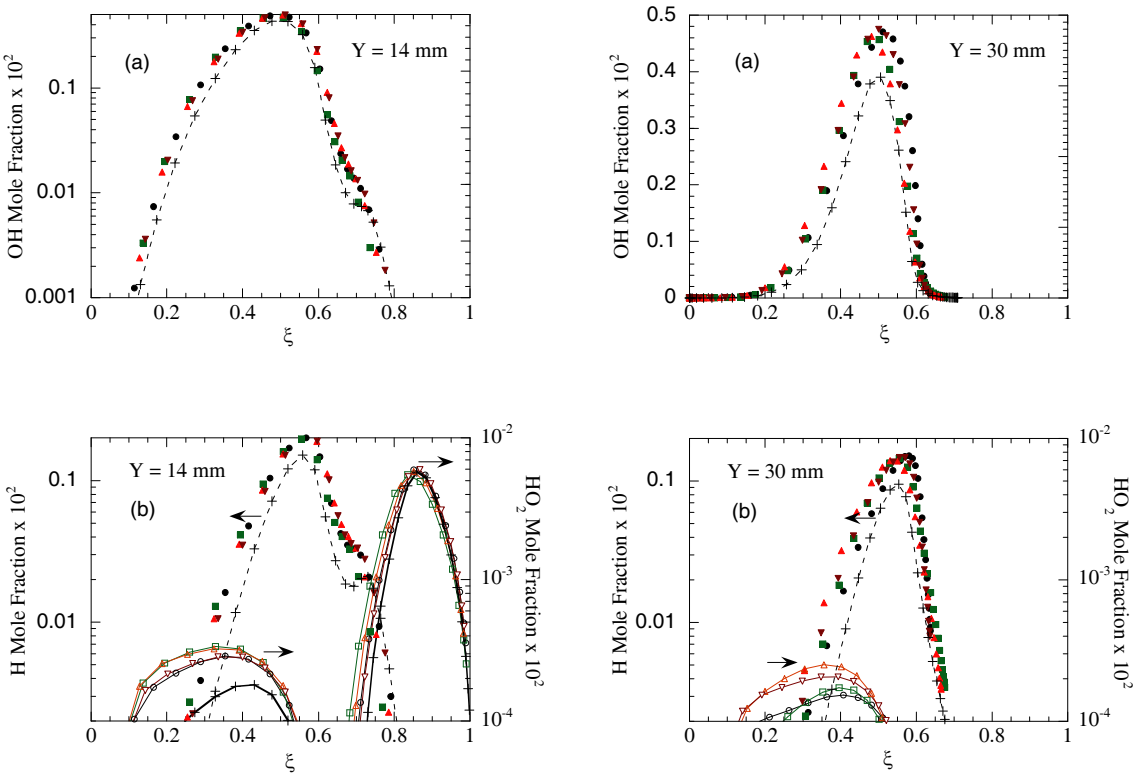
(a)
Y = 14 mm
OH Mole Fraction x 10^2
ξ
(a)
Y = 30 mm
OH Mole Fraction x 10^2
ξ
Y = 14 mm
(b)
H Mole Fraction x 10^2
HO2 Mole Fraction x 10^2
ξ
Y = 30 mm
(b)
H Mole Fraction x 10^2
HO2 Mole Fraction x 10^2
ξ

Figure 10

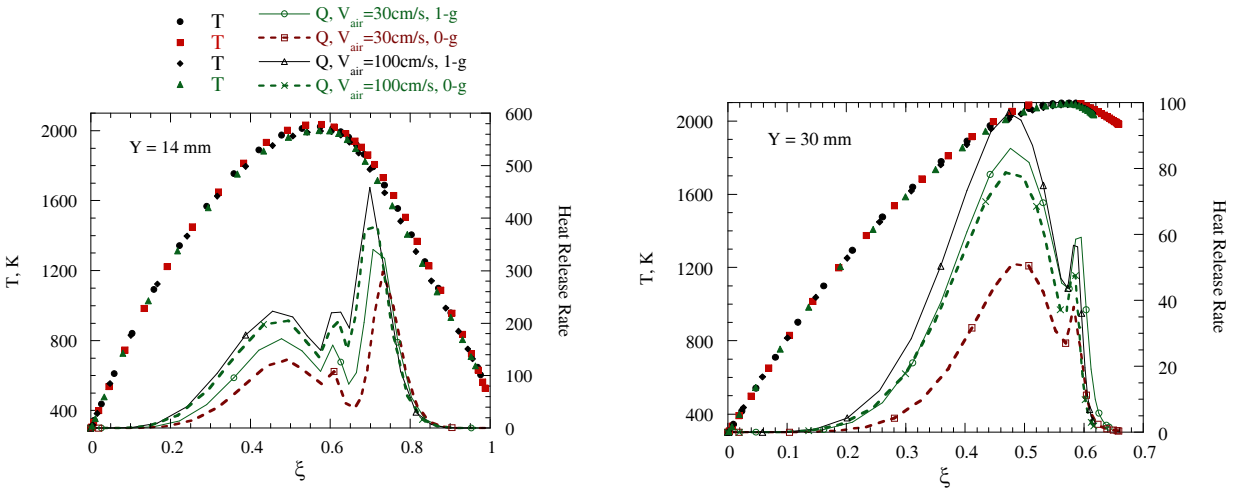
T
T
T
T
Q, V_air=30cm/s, 1-g
Q, V_air=30cm/s, 0-g
Q, V_air=100cm/s, 1-g
Q, V_air=100cm/s, 0-g
Y = 14 mm
Y = 30 mm
T, K
Heat Release Rate
ξ

Figure 11